High-Coherence Hybrid Superconducting Qubit

Matthias Steffen, Shwetank Kumar, David P. DiVincenzo, J. R. Rozen, George A. Keefe, Mary Beth Rothwell, and Mark B. Ketchen

IBM Watson Research Center, Yorktown Heights, New York 10598, USA

(Received 30 April 2010; published 1 September 2010)

We report quantum coherence measurements of a superconducting qubit whose design is a hybrid of several existing types. Excellent coherence times are found: $T_2^* \sim T_1 \sim 1.5$ μs. The topology of the qubit is that of a traditional three-junction flux qubit, but it has a large shunting capacitance, and the ratio of the junction critical currents is chosen so that the qubit potential has a single-well form. The qubit has a sizable nonlinearity, but its sign is reversed compared with most other popular qubit designs. The qubit is read out dispersively using a high-Q resonator in a $\lambda/2$ configuration.

DOI: 10.1103/PhysRevLett.105.100502 PACS numbers: 03.67.Lx, 03.65.Yz, 74.50.+r

While there have been many successful superconducting qubit types, their large diversity suggests that the optimal qubit will be a hybrid combining favorable features of all of the following: the tunability of the flux qubit [1–3], the simplicity, robustness, and low-impedance of the phase qubit [4–6], and the high-coherence and compatibility with high-Q superconducting resonators of the transmon [7,8]. We present here experimental results on such a hybrid, a low-impedance flux qubit (low-Z flux qubit), related to a suggested design of You *et al.* [9]. This qubit has excellent coherence times, comparable to the best currently reported for superconducting qubits. While the design is basically that of a three-junction flux qubit [1], the ratio of junction critical currents is chosen to give the qubit's potential a single-well form.

The key to this qubit is its large shunting capacitance ($C_s = 100$ fF) and therefore its low effective impedance $\sqrt{L_J/C_s}$; this protects the qubit from decoherence. As Fig. 1(a) shows, the shunt capacitor is realized using a simple, reliable single-level interdigitated structure. We choose the ratio of the small and large junction critical currents I_0 to be around $\alpha = 0.3$. For this α the qubit potential has only one minimum [see Eq. (3) below], and the qubit shows only a weak dependence of the qubit frequency ω_{01} on applied flux Φ, where ω_{ij} is the transition frequency between the energy levels i and j. As for the original flux qubit, a "sweet spot" exists at which the qubit is to first order insensitive to Φ, giving rise to long dephasing times, but even away from this degeneracy point our frequency sensitivity is about a factor of 30 smaller than in the traditional flux qubit. Our flux sensitivity is comparable to that of the phase qubit ($\partial\omega_{01}/\partial\Phi \sim 2\pi 30$ GHz$/\Phi_0$) which permits tunability without completely destroying phase coherence, despite the presence of significant flux noise amplitude on the order of $S_\Phi = 1 - 2\mu\Phi_0/\sqrt{\text{Hz}}$. Modeling indicates that our qubit at the sweet spot still has appreciable anharmonicity, with $|\omega_{12} - \omega_{01}|/2\pi$ in the neighborhood of several 100 MHz (or about 2%–10% of the qubit resonance frequency, depending on α), but interestingly, with $\omega_{12} > \omega_{01}$, the opposite of any superconducting qubit except the flux qubit [2] and fluxonium [10]. On-resonance coupled phase qubits or transmons have the noncomputational states $|20\rangle$ and $|02\rangle$ lower in energy than $|11\rangle$, which potentially permits decay mechanisms into these states. With our "inverted" or opposite anharmonicity of the hybrid qubit, coupled hybrid qubits have these noncomputational states at energies higher than that of $|11\rangle$.

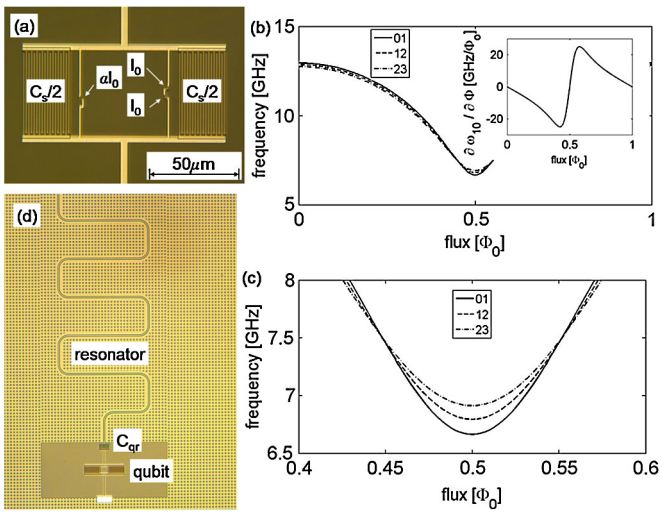

FIG. 1 (color online). Micrograph and simulated frequency response of the low-Z flux qubit. (a) A micrograph of the qubit shows the interdigitated shunting capacitor ($C_s = 100$ fF), which is made of aluminum simultaneously with the junction fabrication step. The qubit has three junctions, as in the traditional flux qubit. (b) The qubit frequency response is much weaker than the traditional flux qubit (inset: derivative $\partial f_{01}/\partial\Phi_0$). Near the sweet spot at $\Phi = 0.5\Phi_0$ the qubit anharmonicity is inverted: $\omega_{12} > \omega_{01}$. Simulation parameters are $C_s = 100$ fF, $I_0 = 0.3$ μA, and $\alpha = 0.3$. (d) The qubit is read out dispersively by coupling it capacitively via $C_{qr} \sim 1.6$ fF to a half-wavelength coplanar waveguide resonator with a resonance frequency of $f_r = 10.35$ GHz.

The reduced impedance of this qubit has several advantages. Qubits with low self-capacitance are more susceptible to residual capacitive coupling effects [11,12]. By increasing the self-capacitance to a level similar to the phase qubit and the transmon, these effects are still present but at a more manageable level. Additionally, by introducing a large self-capacitance we provide additional means of coupling multiple qubits effectively (capacitive or inductive coupling).

The low-Z flux qubit is modeled as in Ref. [9]. Assuming the loop inductance is much less than the junction inductance $L \ll L_J$, the potential energy is two dimensional; in terms of sum and difference phases $\delta_{p,m}$,

$$U_{2D} = -2E_J \cos(\delta_p/2)\cos(\delta_m/2) - \alpha E_J \cos(2\pi\Phi/\Phi_0 - \delta_m). \quad (1)$$

Here $E_J = I_0\Phi_0/2\pi$ and $\Phi_0 = h/2e$. The kinetic term is

$$K_{2D} = \left(\frac{\partial}{\partial\delta_p}\right)^2 \frac{4e^2}{C_J} + \left(\frac{\partial}{\partial\delta_m}\right)^2 \frac{4e^2}{C_J(1+2\beta)}, \quad (2)$$

where $\beta = \alpha + C_s/C_J$. C_J is the capacitance of the larger Josephson junctions (typical value is ~5–10 fF for shadow evaporated junctions with an area of about 0.1 μm^2); we assume that the capacitance of the small junction is αC_J. The introduction of a large shunting capacitance $C_s \gg C_J$ permits the δ_p direction to be safely ignored, as confirmed by a Born-Oppenheimer analysis [13]. Thus the potential is accurately represented in a simple one-dimensional form:

$$U_{1D} = -2E_J \cos(\delta/2) - \alpha E_J \cos(2\pi\Phi/\Phi_0 - \delta). \quad (3)$$

Only the second kinetic term remains from Eq. (2) with an effective capacitance approximately equal to C_s. The expected frequency dependence of the first four energy levels is shown in Figs. 1(b) and 1(c) as well as the derivative (inset). We note that because the potential has only one minimum, it is not practical to measure the state of the low-Z flux qubit using a magnetometer—but it is quite practical to probe it dispersively via a cavity [7,14].

We fabricated a low-Z flux qubit (closely following steps outlined in [15]) on a 200 mm high resistivity (>1000 Ω cm) silicon (Si) wafer without any thermal oxide. The feed line and resonator as well as the corresponding ground plane are made of 200 nm thick niobium and deposited by physical vapor deposition. The patterning is done using deep UV lithography followed by a reactive ion etch in a chlorine based plasma. Intrinsic quality factors of resonators made separately (10 μm center strip width, 6 μm gap) are measured to be $Q = 8\times10^4$–10^5, confirming clean substrates, and confirming that processing does not introduce significant defects. The Josephson junctions require a second mask, which is created out of a LOR5A/Ge/PMMA trilayer which is patterned by e-beam lithography, then developed, and then etched using a CF_4-Ar plasma. The bottom layer is wet etched using OPD7262. The substrate surface is precleaned using an ion mill, followed by depositing two aluminum layers each at a different angle, separated by a brief oxidation of the first layer to produce high quality Josephson junctions. The shunting capacitor is formed during the Al deposition with 2 μm lines and spaces.

We implemented the required dispersive readout techniques as shown in Fig. 2 and measured the qubit [16]; as Fig. 1(d) indicates, the qubit is grounded and end coupled via a coupling capacitor ($C_{qr} \sim 1.5$ fF) to a standard coplanar waveguide resonator, which is in turn capacitively coupled ($C_{rf} \sim 2$ fF) to a feed line, similar to [14]. We first measure the vacuum-Rabi splitting [Fig. 3(a)] and obtain $g = 45$ MHz, consistent with the magnitude of the small coupling capacitance C_{qr}. We note that the cavity quality factor $Q \sim 6\times10^4$ is quite large and increases the cavity's response time, impacting the signal-to-noise ratio in our experiment [17]. The qubit spectroscopy over a broad flux range is shown in Fig. 3(b) and agrees well with the predicted frequencies from Eq. (3) using $I_0 = 0.34$ μA, $\alpha = 0.43$, and $C_s = 110$ fF (dashed line). Zooming in on the sweet spot [Fig. 3(c)] reveals a flux insensitive qubit response corresponding to $\omega_{10}/2\pi = 4.4225$ GHz. At the sweet spot the anharmonicity of the qubit is measured by applying a large microwave drive and observing the two-photon $|0\rangle \rightarrow |2\rangle$ transition, which is higher in frequency than $\omega_{10}/2\pi$, clearly showing the inverted anharmonicity. Separate experiments confirm this by observing Rabi

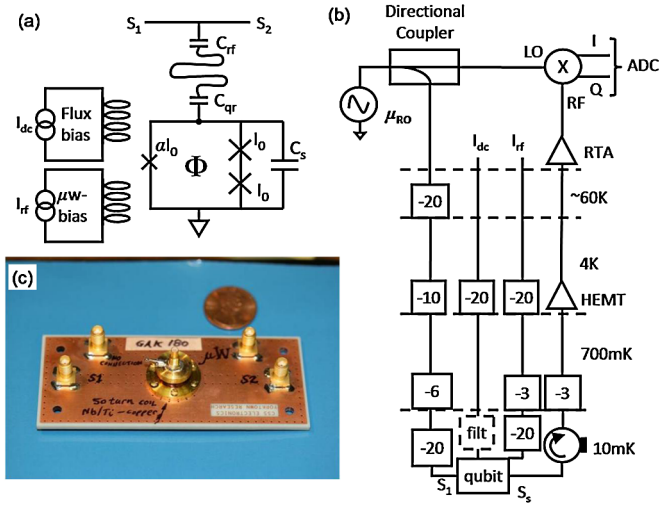

FIG. 2 (color online). Experimental setup. (a) The resonator is capacitively coupled to a feed line. Both the microwaves and dc bias are inductively coupled to the qubit. (b) The qubit is measured dispersively using standard microwave techniques (e.g., [7]). (c) The qubit is mounted on a copper PC board with a high frequency miniature SMA connector. The dc flux bias is generated using a hand-wound external superconducting wire coil mounted on the lid of the box. The microwave bias is supplied by a microwave wire bond on chip that has a small mutual inductance to the qubit loop.

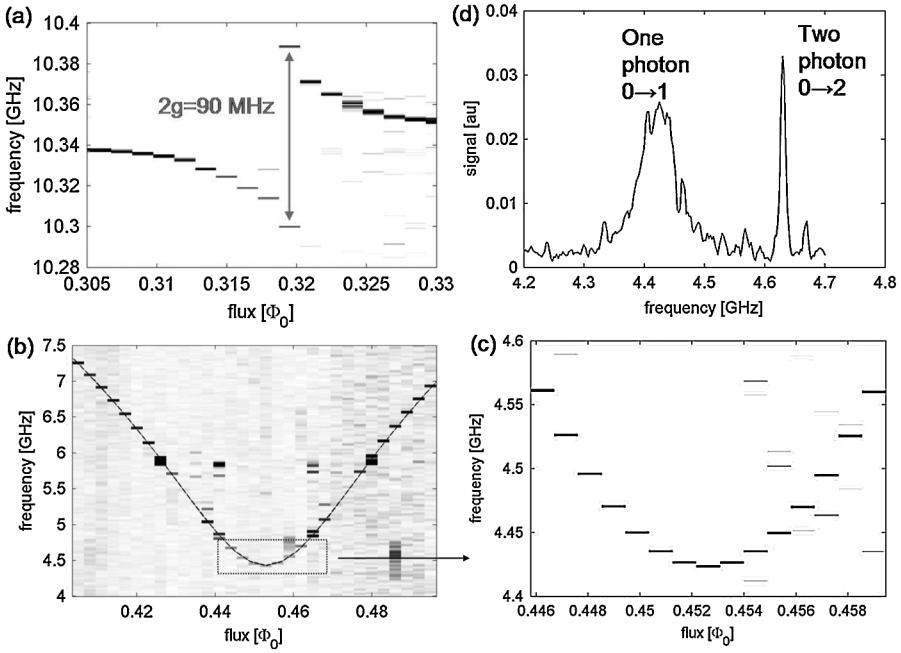

FIG. 3. Qubit spectroscopy. (a) The vacuum-Rabi splitting indicates $g = 45$ MHz. (b) Qubit spectroscopy over a broad flux range agrees well with the one-dimensional theory (dashed line). Because the raw data shows a spectroscopic linewidth of a few MHz it would not be visible on this scale and therefore the data were significantly broadened in software by averaging over 40 MHz to make it visible on this plot. A box mode near 5.6 GHz couples microwaves much more strongly to the qubit than all other frequencies. There is a noticeable offset in flux due to residual magnetic fields in the refrigerator. (c) Qubit spectroscopy near the sweet spot (data not broadened) reminds us of the typical parabolic response of the flux qubit. (d) The two-photon $|0\rangle \rightarrow |2\rangle$ transition is higher in frequency, revealing the inverted anharmonicity of the low-Z flux qubit.

oscillations between the $|1\rangle$ and $|2\rangle$ states, and by identifying a *negative* dispersive shift of the resonator frequency (data not shown). The detuning $(\omega_{12} - \omega_{10})/2\pi \sim 400$ MHz is consistent with parameters obtained from fitting ω_{10} above.

Our low-Z flux qubit has remarkably long coherence times. Figure 4(a) shows a Rabi trace, for various microwave drive amplitudes, indicating a decay constant of nearly 2 μs. A direct measurement of T_1 [Fig. 4(c)], which detects the return of the qubit to the ground state after π pulsing, indicates $T_1 = 1.6$ μs, corresponding to $Q = T_1\omega_{10} = 4.4 \times 10^4$. Figure 4(c) shows a Ramsey spectrum, showing $T_2^* = 1.3$ μs. Refocusing pulses are not used here, but the dc flux is recalibrated back to the sweet spot every few minutes during the experiment to correct for drift. Finally, spin echo data indicate $T_2 = 1.5$ μs (data not included). The fact that $T_2 \neq 2T_1$ indicates dephasing noise is not due to low-frequency but rather to high-frequency fluctuations, possibly in the kHz–MHz regime. Further repeatability studies must be conducted to determine if such noise is consistently present.

The energy decay for a higher qubit frequency $\omega_{10}/2\pi = 7.12$ GHz is found to be $T_1 = 0.86$ μs, corresponding to $Q = 3.85 \times 10^4$, not very different from the measured value at the sweet spot. Dissipation from dielectric loss predicts a frequency independent quality factor, and hence we believe that the energy decay is limited by dielectric loss, presumably in the native oxide formed on the aluminum of the interdigitated capacitor [18]. Although Q appears to vary slightly, we have not performed an exhaustive search to extract Q over all frequencies. $Q = 4 \times 10^4$ is close to the reported value for the transmon (Q near 7×10^4 [19]), which is also suspected to be set by dielectric loss.

As for all other superconducting qubits, the low-Z flux qubit permits the anharmonicity, resonance frequency, and flux sensitivity to be traded off against each other. Such a trade-off optimization is particularly interesting when introducing a tunable ratio α of the critical currents by replacing the small junction with a SQUID [12,15]. Although such an optimization is not the goal in this first demonstration, we believe that the low-Z flux qubit can be made to retain the inverted anharmonicity yet still be tunable with a very weak dependency of the frequency on flux. The rich physics allowed by introducing additional junctions together with the increased self-capacitance is a promising avenue for designing highly scalable qubits.

Several features are clearly to be improved in further experiments. The coupling to the qubit here is set to be very weak, so that the dispersive shift used in the detection is very small (~40 kHz) and the qubit state cannot be acquired in a single shot. Modest increases of the coupling capacitances should permit much reduced averaging times, possibly leading to single-shot readout [20].

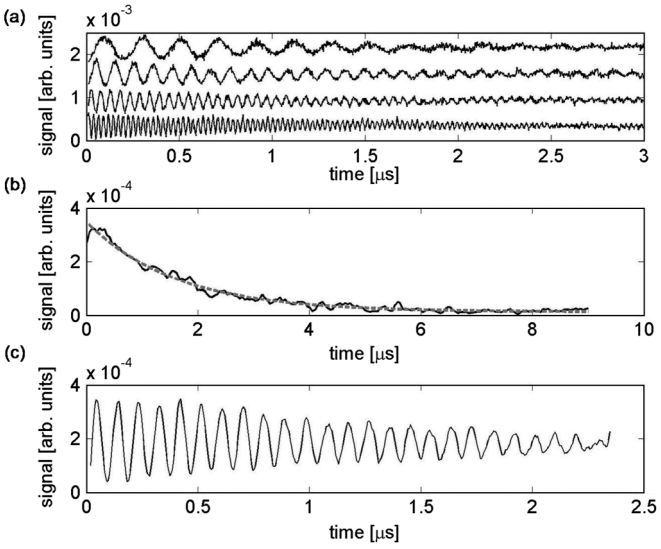

FIG. 4. Coherence time measurements of the qubit. (a) Rabi oscillations. Each trace varies in microwave amplitude by a factor of 2, and we find the Rabi frequency scales accurately with amplitude. (b) A direct measure of the energy decay is obtained from a fit to the data (gray dashed line) and is found to be $T_1 = 1.6$ μs. (c) Ramsey fringes are implemented by applying a Hadamard gate (180° rotation around an axis tilted by 45° from the horizontal axis). The detuning between the qubit and microwave frequency is ~10 MHz, consistent with the observed period. The data can be fitted to an exponential decay with a decay constant $T_2^* \sim 1.3$ μs.

Further spectroscopy studies should confirm interesting qubit bias points, particularly those for which some of the energy transitions are degenerate (e.g., $\omega_{01} = \omega_{12}$ or $\omega_{12} = \omega_{23}$). Quantum information applications using such degeneracies have not been considered much for superconducting qubits because they have not been present thus far. We believe such interesting degeneracies may open the door to build simple superconducting qutrits. Still, the present experiments already tell us a wealth of new information about capacitively shunted qubits. Feared decoherence mechanisms such as dielectric loss, two-level systems, and quasiparticle dissipation still readily permit coherence times at the 1 μs level.

We would like to acknowledge BBN for their help in this effort.

[1] J. E. Mooij *et al.*, Science **285**, 1036 (1999).
[2] I. Chiorescu *et al.*, Science **299**, 1869 (2003).
[3] A. O. Niskanen *et al.*, Phys. Rev. B **74**, 220503 (2006).
[4] M. Ansmann *et al.*, Nature (London) **461**, 504 (2009).
[5] M. Hofheinz *et al.*, Nature (London) **459**, 546 (2009).
[6] M. Steffen *et al.*, Science **313**, 1423 (2006).
[7] L. DiCarlo *et al.*, Nature (London) **460**, 240 (2009).
[8] J. Koch *et al.*, Phys. Rev. A **76**, 042319 (2007).
[9] J. Q. You *et al.*, Phys. Rev. B **75**, 140515 (2007).
[10] V. E. Manucharyan *et al.*, Science **326**, 113 (2009).
[11] M. Steffen *et al.*, New J. Phys. **11**, 033030 (2009).
[12] F. G. Paauw *et al.*, Phys. Rev. Lett. **102**, 090501 (2009).
[13] D. P. DiVincenzo, F. Brito, and R. H. Koch, Phys. Rev. B **74**, 014514 (2006).
[14] M. Steffen *et al.*, Appl. Phys. Lett. **96**, 102506 (2010).
[15] M. Steffen *et al.*, J. Phys. Condens. Matter **22**, 053201 (2010).
[16] For simplicity we are implementing an amplitude measurement $|S_{21}|$ to observe the cavity frequency shift, and have not optimized the setup for maximum signal to noise. The measurement pulse is 8 μs long, and the experimental repetition time is 20 μs. From our data there is no clean method to extract excited state occupation probability with small error bars.
[17] A. Blais *et al.*, Phys. Rev. A **69**, 062320 (2004).
[18] J. M. Martinis *et al.*, Phys. Rev. Lett. **95**, 210503 (2005).
[19] A. Houck *et al.*, Quant. Info. Proc. **8**, 105 (2009).
[20] M. D. Reed *et al.*, arXiv:1004.4323.